Available online at www.sciencedirect.com
SCIENCE DIRECT®

Mechanics of Materials 35 (2003) 313–331

MECHANICS OF MATERIALS

www.elsevier.com/locate/mechmat

Cleavage cracking resistance of high angle grain boundaries in Fe–3%Si alloy

Y. Qiao, A.S. Argon *

Department of Mechanical Engineering, Massachusetts Institute of Technology, 77 Massachusetts Avenue, Cambridge, MA 02139-4307, USA

Received 20 July 2001; received in revised form 20 February 2002

This paper is dedicated to Sia Nemat-Nasser on his 65th birthday in recognition of his many outstanding contributions to the mechanics of materials

Abstract

High angle grain boundaries in steel offer an important resistance to the propagation of cleavage cracks that affects the fracture toughness and can modulate the ductile-to-brittle transition temperature of fracture downward. This behavior has been studied now in bicrystals of Fe–3%Si alloy in detail. It was noted that the twist misorientation across a high angle boundary has a more profound effect on cleavage fracture resistance than the tilt misorientation. Specific measurements of such resistance over a random selection of high angle grain boundaries in bicrystals and associated fractographic studies have led to quantitative models of the resistance that high angle grain boundaries offer to cleavage cracks. The study has also revealed a transition from pure cleavage to mixed cleavage around 0 °C for this alloy above which the observed definite increment of fracture work could be associated with the sigmoidal plastic bending and rupture of ligaments left between separate cleavage strips in the adjoining grain.

Keywords: High angle grain boundaries; Cleavage resistance of boundaries; Fe–3%Si alloy

1. Introduction

The subject of high angle grain boundaries and their role in affecting the plastic resistance and fracture behavior of polycrystals has been of continued interest. In either case, grain boundaries compartmentalize processes in individual grains and break up both slip operations and limit the propagation of cleavage cracks from grain to grain. Their roles in affecting the plastic resistance of polycrystals, starting from considerations of initial yielding behavior (Hall, 1951; Petch, 1953) to introducing intercrystalline constraints that influence compatibility of deformation between grains have been actively explored over the years, but are not of interest to us here. In many respects the role of grain boundaries in fracture is far wider in terms of phenomena than their role in modulating plastic deformation. Among the many

* Corresponding author. Tel.: +1-617-253-2217; fax: +1-617-258-5802.
E-mail address: argon@mit.edu (A.S. Argon).

0167-6636/03/$ - see front matter
PII: S0167-6636(02)00284-3

effects of grain boundaries on fracture, including initiation of microcracks by arrest of slip bands (Zener, 1949; Stroh, 1954, 1955) or deformation twins (Hull, 1960), and triggering of cleavage fracture through the cracking of grain boundary carbides (McMahon and Cohen, 1965; Knott and Cottrell, 1963; Ritchie et al., 1973; Knott, 1997), here we are interested primarily in the role of grain boundaries in modulating cleavage cracking across grain boundaries.

In an early fundamental experimental study of the processes that lead to transitions of fracture from ductile-to-brittle forms in polycrystalline steel Hahn et al. (1959) noted that with decreasing temperature and rapidly increasing plastic resistance, prior to the onset of full brittleness, slip induced dormant grain sized microcracks appear. This demonstrated clearly that in the initiation of brittle response while microcrack nucleation by obstructed slip or twining processes is an important precursor, such microcracks have to break-through grain boundaries to initiate global brittle behavior, indicating that grain boundaries offer an important resistance to propagation of cleavage cracking among grains in the nature of acting as "fire breaks". It is this particular role of high angle grain boundaries in affecting cleavage cracking resistance which retards brittleness that is of primary interest here. While this behavior has been well appreciated, definitive studies of the effect to ascertain the nature of this fracture resistance in intrinsically brittle materials is rare. The few definitive studies have been limited to the assessment of such resistance by individual grain boundaries with known lattice misorientation, in hydrogen charged Fe–3%Si alloy by Gell and Smith (1967) and to some models considering such resistance by Anderson et al. (1994), Crocker et al. (1996) and McClintock (1997).

In the present study we have explored in considerable detail the particular forms of processes that affect the break-through of cleavage cracks across specific grain boundaries with known misorientation of tilt and twist across them and how this governs the specific levels of resistance to cleavage crack propagation across grain boundaries in both its topological features and its kinetics, leading to specific models of such resistance. In a companion study we have broadened the observations and the models to the resistance of cleavage cracking through a field of grain boundaries in both homogeneous Fe–2%Si alloy as well as homogeneous (free of pearlite) low carbon steel (Qiao and Argon, 2003).

2. Experimental details

2.1. Material

The principal thrust in the present research was the elucidation of the effect of high angle grain boundaries on the resistance to cleavage crack growth in iron and steel. This was pursued by a detailed study of the effect in a substantial set of bicrystals with a wide range of lattice misorientation. The pursuit became possible through the donation of a large ingot of Fe–3%Si alloy by the Allegheny Ludlum Steel Co. In the slowly cooled ingot of about 12 cm thickness the size of grains ranged from roughly 5 mm diameter on the surface to about 50–80 mm in the interior. The chemical composition by weight of the material as given in Table 1 indicates a substantial carbon content.

Metallographic examination of the microstructure of the as-received ingot revealed a high concentration of very large size elongated carbides, ranging in size from 10 μm to fractions of a millimeter, and with the carbide size increasing with increasing grain size. In addition a high concentration of ubiquitous narrow deformation twins were also found in most of the possible variants. Preliminary cleavage studies of grains indicated quite significant perturbations to the growth of cleavage cracks by the narrow deformation twins and to a much lesser extent by the carbides. Nevertheless, the carbides were removed by a special two step schedule of decarburization of the material to be described below. Predictably, the deformation twins proved quite resistant to removal by any meaningful heat treatment.

Table 1
Chemical compositions of the Fe–3%Si ingots as-received

Elements	C	Si	S	P
Content in weight (%)	0.63	3.4	<0.01	<0.01

2.2. Material preparation

2.2.1. Harvesting of bicrystals from the ingot

The entire set of bicrystals used in this investigation were harvested from a special block of a Fe–3%Si alloy ingot. The block of roughly 12 cm thickness had lateral dimensions of 30 × 40 cm. Out of this block 2 slices of ≈6 mm thickness were cut across the thickness direction of the block. The slices were surface ground to a fine finish. By virtue of the large grain sizes in the ingot many grains in the slices were of a through-thickness nature. The surface-ground slices were etched in 3% *nital* for ≈24 h to reveal the low energy (1 0 0) facets in the large collection of grains contained in the slice. Most grains, being randomly oriented in relation to the ground surface of the slice, produced pyramidal etching facets representing corners of cubes of {1 0 0} type planes. There were, however, also grains which exhibited only sets of two etching facets indicating that such grains contained one of their ⟨1 0 0⟩ directions lying in the ground surface. Finally, there were several quite large grains of 25–30 mm diameter which contained no etching facets but only a set of shallow etch pits with flat bottoms, signifying that these grains had one of their {1 0 0} planes lying parallel the surface of the slice and containing two mutually perpendicular {1 0 0} planes perpendicular to the surface of the slice as depicted in the sketch of Fig. 1. These grains with their adjoining family of attached smaller grains were candidates for extraction of bicrystals. X-ray Laue back-reflection analysis confirmed the accuracy of this method of determination of grain orientation by etching. Upon identification of the desired central grain, it and its surrounding grains were removed from the large slice by electrical discharge machining (EDM). The large properly oriented central grain was identified as A. Further EDM sectioning parallel to one or the other of the ⟨1 0 0⟩ type directions of grain A across its boundary into the surrounding grains then furnished a set of bicrystal pairs A and B. Since two adjacent slices of the ingot contained further extensions of grains A and most of the surrounding B grains, a number of identical prismatic bicrystal pairs could also be harvested which were utilized in repeating some experiments or to explore the temperature dependent response of identical bicrystal pairs. The orientations of the surrounding B grains were all obtained by X-ray Laue back-reflection analysis.

2.2.2. Characterization of lattice misorientations of surrounding grains

As will become clear from our experimental results to be presented in Section 3, the form of interaction of a cleavage plane with a grain boundary and its penetration into the adjacent grain B is governed primarily by the tilt and twist misorientations of the adjoining grain across the grain boundary, (see also Gell and Smith, 1967). The angles of tilt ψ, and twist φ of grain B across the grain boundary plane, relative to grain A can be given as (Fig. 2),

$$\psi = \frac{\pi}{2} - a\cos(\alpha_{31}\sin\beta + \alpha_{32}\cos\beta) \qquad (1a)$$

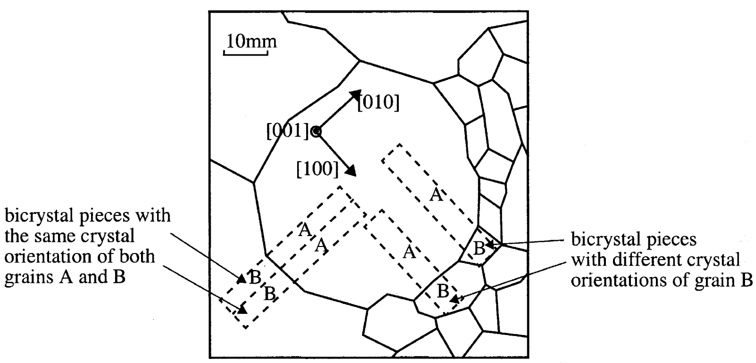

Fig. 1. Sketch demonstrating the method of harvesting bicrystals from an Fe–3%Si alloy ingot containing large grains.

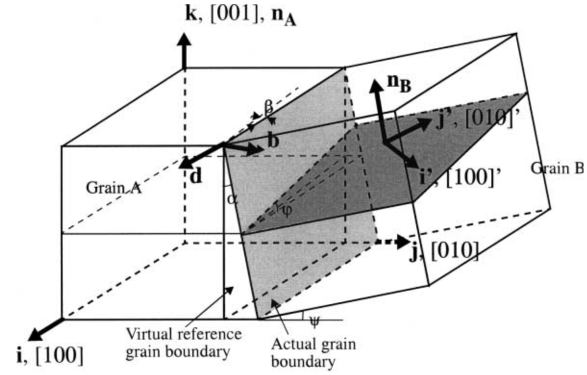

Fig. 2. Determination of lattice tilt and twist misorientations across a grain boundary in a bicrystal.

$$\varphi = \frac{\pi}{2} - a\cos(\alpha_{31}\cos\beta + \alpha_{32}\sin\beta) \tag{1b}$$

in Eqs. (1a) and (1b) α_{31} and α_{32} are the direction cosines locating the unit normal vector **n** of the principal cleavage plane of grain B relative to the axes **i** and **j** of grain A, parallel to the [1 0 0] and [0 1 0] directions respectively of that grain; and where β is the angle between a vector **d**, parallel to the line of intersection of the grain boundary with the principal cleavage plane (0 0 1) of grain A and its [1 0 0] direction as shown in Fig. 2 (Appendix A). Ideally, the angle β should have been zero, but could not be controlled in the experiments. As the fractographs show it was often in the range of 20–30°, without any significant effect on the mechanisms discussed in Section 3. While the inclination of the plane of the grain boundary also requires an angle α giving the rotation of the plane of the boundary about the vector **d** in the boundary, this degree of freedom is considered inessential since the interaction of the cleavage crack in grain A with the grain boundary in its traverse into grain B is primarily governed with respect to a virtual boundary perpendicular to the cleavage plane ($\mathbf{n}_\mathbf{A}$). Through the form of preparation of the bicrystals it was possible to obtain 17 different bicrystal pairs with relatively random distribution of tilt and twist angles ψ and φ of grain B relative to the boundary planes with grain A. The different tilt and twist angles of these 17 different bicrystals are given in Table 2.

Table 2
Characteristics of the 17 bicrystal samples: measured values of $K_{\mathrm{ICGB}}/K_{\mathrm{ICA}}$ and normalized experimental and computed toughness compared

	Sample																
	1	2	3	4	5	6	7	8	9	10	11	12	13	14	15	16	17
ψ	0.175	0.210	0.331	0.157	0.140	0.122	0.140	0.594	0.229	0.402	0.052	0.385	0.210	0.367	0.490	0.524	0.280
φ	0.559	0.052	0.245	0.367	0.332	0.734	0.069	0.210	0.455	0.699	0.052	0.297	0.227	0.455	0.245	0.069	0.542
$K_{\mathrm{ICGB}}/K_{\mathrm{ICA}}$	1.461	1.049	1.168	1.226	1.192	1.575	1.042	1.233	1.283	1.602	1.036	1.225	1.141	1.404	1.204	1.121	1.425
$(\Delta K_{\mathrm{ICGB}})_{\mathrm{E}}/(\Delta K_{\mathrm{ICGB}})_{\mathrm{C}}$	1.132	0.942	0.977	0.967	1.046	1.096	0.964	0.984	1.030	0.923	1.002	0.995	1.000	1.078	0.969	0.921	1.073

2.2.3. Decarburization of bicrystals

To eliminate the complicating and undesirable interactions of cleavage cracks with the large carbides all bicrystals were decarburized according to a stringent schedule (Birks, 1969; Thelning, 1984). The schedule consisted of first breaking-down the carbides by a prolonged period (60 h) of soaking of the bicrystals at 1400 °C in a nitrogen environment which successfully dissolved all carbides. This treatment was followed without interruption by a holding time of 2.5 h at 1200 °C in a hydrogen environment to extract the dissolved carbon. The schedule ended with a slow furnace cooling to prevent entrapment of hydrogen and embrittlement. The remaining carbon in the decarburized bicrystals was less than 0.1% by weight and entirely in solution. A final *picral* etch detected no carbides in the grains. There was no measurable change in the Si content as a result of the decarburization treatment. As expected, the prolonged decarburization treatment had no effect on the population of the narrow deformation twins.

2.2.4. Welding of bicrystals into double cantilever beam "carrier" samples

The average size of the harvested and decarburized bicrystal slabs was 40 × 10 × 4 mm. These were electron-beam welded into fine grained 1020 steel carriers according to a special welding procedure to minimize residual stresses in the construction of the double cantilever beam (DCB) specimens. The procedure is depicted in Fig. 3 showing the five separate welding paths to attach the bicrystal slabs to the three 1020 steel blocks (always individually produced for each bicrystal) with minimal distortion. The unwelded space between blocks I and II becomes the main part of the initial crack. After welding, the DCB specimens were stress relieved at 400 °C for 2 h, and subsequently surface ground to a final thickness of somewhat under 4.0 mm. To reduce the risk of cleavage cracks turning out of the desired median plane, shallow side grooves of 60° angle were machined by a special cutter with a contoured tip. The combined depth of the side grooves reduced the central ligaments of the DCB samples to b_n roughly 3.0 mm. At the tip of the crack, grain A, was provided with a 45° chevron by EDM milling. In this manner 17 DCB samples were prepared for the first phase of the investigations at −20 °C.

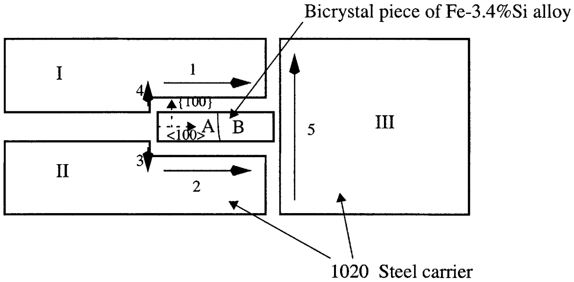

Fig. 3. Schedule of assembly by EB welding of bicrystal slabs into 1020 steel carrier blocks to form DCB specimens.

2.3. Single crystal tension tests

Single crystal tension specimens were cut out from a single large grain to carry out stress–strain experiments to determine the temperature dependence of the plastic resistance of the material of interest for reference. These specimens had not been decarburized since the remaining carbon in the material outside the carbides was at the solubility limit and that the relatively small volume fraction of the large carbides would affect the plastic resistance only to a minor extent. The Schmid factor for the principal $\{1\,1\,0\}\langle 1\,1\,1\rangle$ type slip system was 0.44 while that for the alternative $\{1\,1\,2\}\langle 1\,1\,1\rangle$ system was 0.37. Because of the low temperatures in the test and the higher Schmid factor, the $(1\,1\,0)[1\,\bar{1}\,1]$ system was taken to be the active one in the evaluation of the plastic glide resistance.

2.4. The wedge-loading test configuration

To achieve the best conditions of propagating the cleavage cracks to probe the grain boundaries in the bicrystals, a stiff loading arrangement having a minimal compliance C_m was devised which is shown schematically in Fig. 4. The DCB specimen containing the specific embedded bicrystal was pried apart by means of a hardened steel wedge

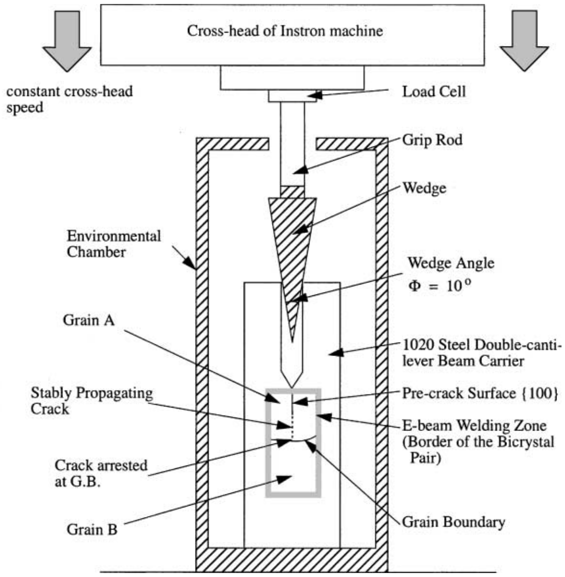

Fig. 4. Arrangement to perform wedge-loaded crack propagation experiments in DCB samples.

with a wedge angle of 10°. To reduce friction between the DCB specimen slab and the wedge, both contacting surfaces were covered with a graphite spray. The wedge was driven-in by the cross-head of a type 5508 Instron machine. The wedge insertion load was measured by a type LW0-300 flat compression load cell, having a compliance, $C_{lc} = 1.86 \times 10^{-11}$ m/N given by the manufacturer, Transducer Techniques Inc. The loading rod, made out of solid stainless steel was kept as short as possible. The measured overall compliance C_m of the loading system was 9.0×10^{-8} m/N which was roughly 1% of the opening compliance of a typical DCB specimen.

The environmental chamber made up of aluminum sheet metal with an external layer of Styrofoam insulation, contained a Plexiglas window to view the specimens. The temperature in the chamber was maintained directly by a stream of cold nitrogen gas, fed into the chamber, and was controlled at a desired set-point by an Omega JK12 controller through a cryogenically rated solenoid valve in the liquid nitrogen piping system. Temperature uniformity in the specimen, in equilibrium with its surroundings, was reached typically within 15 min.

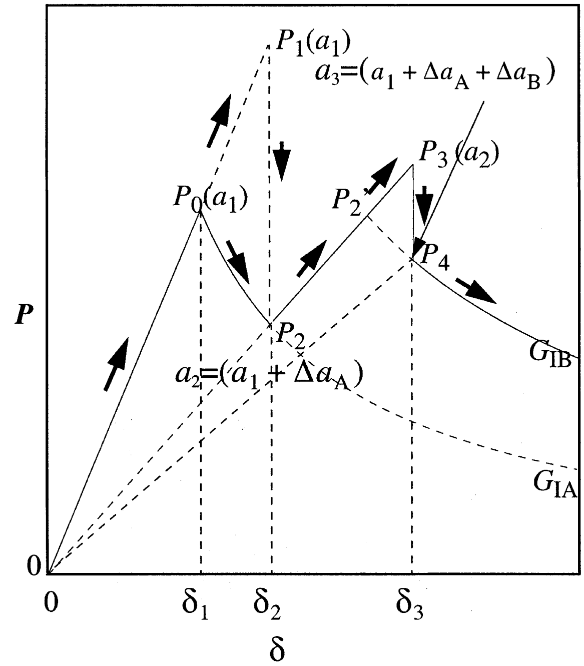

Fig. 5. Idealized opening load, P, vs. opening displacement, δ, response characteristic of the DCB specimen in a "reversible" manner.

2.5. The ideal wedge-loading experiment

Fig. 5 represents the idealized response of the DCB specimen to the propagation of a cleavage crack across a single grain boundary in a bicrystal. While the actual behavior always differed from the idealized one, the latter serves to give a well defined framework to evaluate the response in a quantitative manner.

In the ideal response the crack in grain A begins to grow when the load reaches P_0 at the opening displacement δ_1 where the elastic energy release rate from the DCB specimen equals the specific work of fracture G_{ICA} of grain A (or its critical energy release rate) following a characteristic descent curve P vs. δ, given by:

$$P = D\frac{G_{ICA}^{3/4}}{\delta^{1/2}} \tag{2}$$

where $D = (Eh^3)^{1/4}(b/8)(16/3)^{3/4}$ is a constant of the DCB specimen, where b is the DCB specimen thickness, and h is the height of its arm.

The crack grows by Δa_A until it encounters the grain boundary at a load P_2 and opening displacement δ_2. The area (OP_0P_2) of the P vs. δ diagram represents the work of crack extension by Δa_A, giving an estimate for G_{ICA}:

$$G_{ICA} = \frac{\mathrm{Area}(OP_0P_2)}{b_n \Delta a_A} \tag{3}$$

where b_n is the thickness of the DCB specimen across the roots of the side grooves. At this point the cleavage crack probes the grain boundary and begins to penetrate into grain B in which by virtue of its misorientation, and for reasons to become clear by the fractographic evidence described in Section 3, the specific work of fracture in grain B, G_{ICB}, (in terms of crack growth in the median plane of the DCB specimen) is larger than G_{ICA}. Thus, to initiate a further extension of the crack from a length of $(a_0 + \Delta a_A)$ requires a load increase along line OP_2 to past point P_2', to point (P_3, δ_3) where the peak grain boundary penetration resistance is reached and the crack advances under an excess driving force into grain B by an amount Δa_B in a sudden jump, accompanied by a characteristic load drop $\Delta P = P_3 - P_4$. During this crack jump a certain work W_{GB} of breaking-through the GB is coupled with an increment of work of fracture of grain B over the crack growth increment of Δa_B. In Fig. 5 the former is represented by the area ($P_2'P_3P_4$) while the latter with area ($OP_2'P_4$). In the experimental evaluation of the resistance of grain boundaries the above separation of the effect into work of boundary break-through and cleavage crack propagation in grain B was not made and the entire effect was evaluated simply by defining the stress intensity increment ΔK_{ICGB} based on $\Delta P' = P_3 - P_2$ of Fig. 5 representing the collective actions of the resistance of the GB to break-through.

In the actual wedge-loading experiment the initial penetration of the cleavage crack into grain A is not quasi-static but always requires an excess of "driving force" indicated by the dotted rise of load to P_1 due to a variety of imperfections at the initial crack tip. The crack then jumps through grain A under decreasing load ($P_1 \rightarrow P_2$) until it is stopped at the grain boundary.

3. Experimental results

3.1. Single crystal experiments

The temperature dependence of the tensile yield stress and the critical resolved shear stress on the primary $\{1\,1\,0\}\langle 1\,1\,1\rangle$ system and the alternative $\{1\,1\,2\}\langle 1\,1\,1\rangle$ system is given in Fig. 6. The plastic glide resistance (the CRSS) rises from a plateau of around 150 °C from a level of 80 MPa with increasing slope to a substantial level of 240 MPa around −50 °C. The higher temperature plastic resistance at 150 °C is most likely governed by the solid solution strengthening of the 3% Si. The rise below 50 °C is attributed to a combination of lattice resistance and solid solution resistance. The low temperature plateau below −50 °C and the quite erratic behavior there is attributed to an onset of deformation twinning. Fig. 6 also shows a corresponding rise in the fracture stress which below −50 °C is far less affected by twinning. For our modeling discussed in Section 4 below, we are interested in CRSS on the $\{1\,1\,0\}\langle 1\,1\,1\rangle$ system.

3.2. Bicrystal fracture experiments at −20 °C

Fig. 7a shows the dependence of the DCB opening force P on the associated crack opening

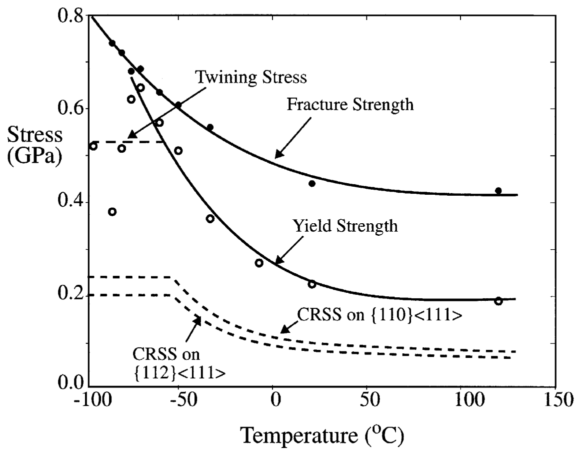

Fig. 6. Temperature dependence of the tensile yield strength, tensile fracture strength, and critical resolved shear stresses on the $\{1\,1\,0\}\langle 1\,1\,1\rangle$ and $\{1\,1\,2\}\langle 1\,1\,1\rangle$slip systems on single crystal tensile tests of the Fe–3%Si alloy. The dotted horizontal line through the region of scatter reflects an approximate level of twining-controlled yielding.

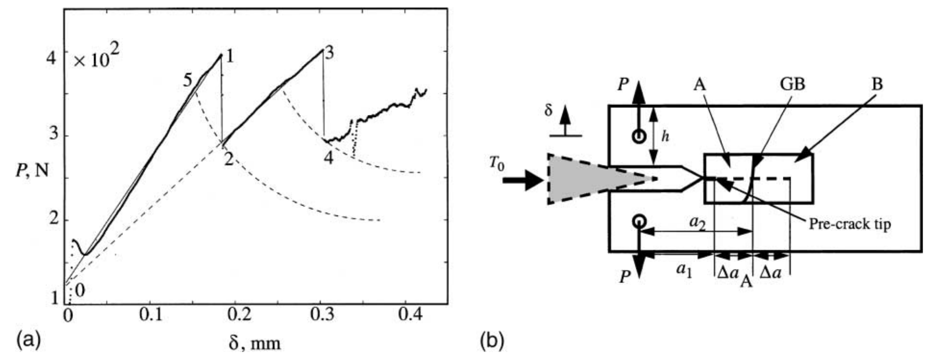

Fig. 7. (a) An actual $P(\delta)$ curve for a wedge-loading experiment of a DCB sample depicted in (b).

displacement δ at the contact point of the wedge in a typical experiment. Because the crack tip was imperfect as produced, the crack propagation was not of a quasi-static nature as outlined in Section 2.5. In the figure the solid contour represents the recorded experimental data while the dashed curves are the fitted ideal response characteristics that resemble those discussed in Section 2.5. During the load rise from 0 to 1 the crack, of length a_1 in Fig. 7b elastically flexes, exerting an increasing stress intensity. At a point past 5 of the initial DCB flexure line the crack begins to grow across the chevron, indicated by the slight decrease of the loading slope. Because of crack tip imperfections the crack becomes overstressed to reach a K_I level exceeding somewhat the K_{IC} for quasi-static growth. At point 1, K_I for initiation of crack growth is reached, the overstressed crack jumps in an unrestrained manner across grain A and comes to rest at the grain boundary. At this stage the crack probes the grain boundary and, in a way that will become clear from the SEM observations, it begins to penetrate partially into grain B, but a full penetration requires an increase in the crack "driving force" K_I along a new loading line with smaller slope due to the increased compliance. When point 3 is reached, under the increment ΔK_I, the crack breaks-through the grain boundary and penetrates into grain B by a further unstable jump. The crack comes to rest on the opposite border of grain B with the polycrystalline background, i.e., at point 4. The subsequent serrated loading behavior past point 4 conveys no relevant information.

The curve of Fig. 7a shows that frictional effects are still present between the wedge and the contacting faces in the DCB specimen, demonstrated by the fact that the loading does not start from zero but from a finite resistance. This artifact is formally rectified by shifting the origin of the loading curves to zero.

From basic beam theory the stress intensity probing the crack tip in grain A at the start can be stated as

$$K_I = \Gamma P a \tag{4}$$

where

$$\Gamma = \sqrt{\frac{12}{(1-\nu^2) b b_n h^3}} \tag{5}$$

in which P is the applied DCB opening load with an initial crack length of a_1 and the other quantities are as defined in Section 2.5. Thus, the initial crack growth resistance K_{ICA} for grain A, then is:

$$K_{ICA} = \Gamma P_1 a_1 \tag{6}$$

where a_1 is the initial crack length and P_1 the critical load to initiate its extension at point (1) in Fig. 7a. The unstable jump of the crack is arrested at point (2), when the crack runs into the grain boundary.

Finally, the stress intensity K_{13} to break-through the grain boundary can be taken similarly to be

$$K_{13} = \Gamma P_3 a_2 \tag{7}$$

where a_2 is the total crack length abutting on the grain boundary. Then, the incremental fracture toughness ΔK_{ICGB} attributable to the grain boundary fracture resistance can be taken as

$$\Delta K_{ICGB} = \Gamma a_2(P_3 - P_2) \tag{8}$$

In this manner altogether 17 bicrystal samples of different lattice misorientations between grains B and A were probed. The resulting measurements of the ΔK_{ICGB} normalized with the overall average K_{ICA} for these 17 bicrystal experiments are given in Table 2 as a function of the individual tilt and twist angles ψ and φ. The overall average of the measured K_{ICA} was 14.1 ± 0.6 MPa $\sqrt{m}$. This value is of substantial magnitude and requires an explanation which we will provide in Section 4.1. Examination of the reported values of K_{ICGB}/K_{ICA} in Table 2 shows a clearly discernable increase with the twist angle φ.

The above development is based on simple beam theory. Somewhat more exact developments are possible, such as that given by Kanninen (1973), but differ in results from the simple theory by less than 5%.

3.3. Fracture transition experiments in bicrystals

To explore how the grain boundary modulates the cleavage cracking across it with changing temperature two sets of additional bicrystal samples were prepared for use in wedge cracking experiments in a temperature range between −20 and 21 °C. In the first set which we label as set "C" it was possible to use six other available bicrystal samples of type "6" in Table 2, i.e., with tilt and twist angles of $\psi = 7°$ and $\varphi = 42°$. For the second set nine bicrystals of a rather different misorientation consisting of $\psi = 8°$ and $\varphi = 12°$ were extracted from the remaining large slice of the same ingot. This set is labeled as "D". The measured K_{ICGB} values normalized with K_{ICA} are listed in Table 3 and are also shown in Fig. 8 as

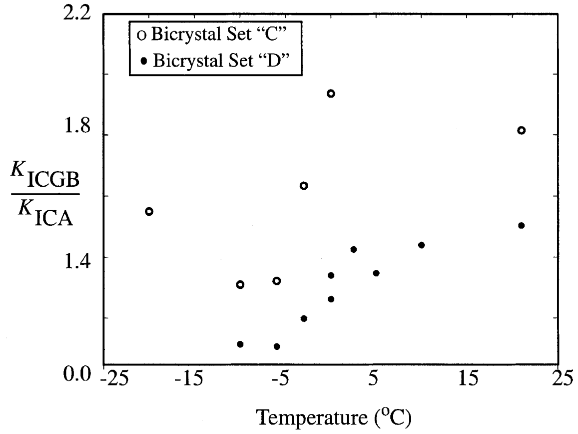

Fig. 8. The temperature dependence of the normalized grain boundary break-through toughness for two special orientations "C" (○) and "D" (●) showing a cleavage to *mixed-cleavage* transition at about 0 °C.

$\Delta K_{ICGB}/K_{ICA}$ over the temperature range, where K_{ICA} is considered temperature independent. The figure shows that there is a readily recognizable transition in the grain boundary cracking resistance between −2 and 0 °C in these two sets. The increment in cracking resistance is distinctly higher in set "C" with the larger twist misorientation angle. The nature of this transition will be clarified with the SEM fractography observations presented in Section 3.4. Since the fracture appearance in the entire temperature range remains to be substantially of a cleavage nature the transition has been labeled as a cleavage to *mixed-cleavage transition*.

3.4. Fractographic observation

3.4.1. Fracture surfaces in grain A

Fig. 9a and b show portions of the cleavage fracture surfaces of grain A at −20 °C for a case

Table 3
Measured normalized K_{ICGB}/K_{ICA} for the two specimen sets of bicrystal experiments carried out in the temperature range of −20 to 21 °C.

T (°C)	−20	−10	−6	−3	0	2.5	5	10	21
Set "C"[a]	1.587	1.312	1.319	1.631	1.936	–	–	–	1.814
Set "D"[b]	–	1.114	1.106	1.199	1.340; 1.262	1.426	1.348	1.440	1.503

[a] Bicrystal set "C" had $\psi = 7°$ and $\varphi = 42°$.
[b] Bicrystal set "D" had $\psi = 8°$ and $\varphi = 12°$.

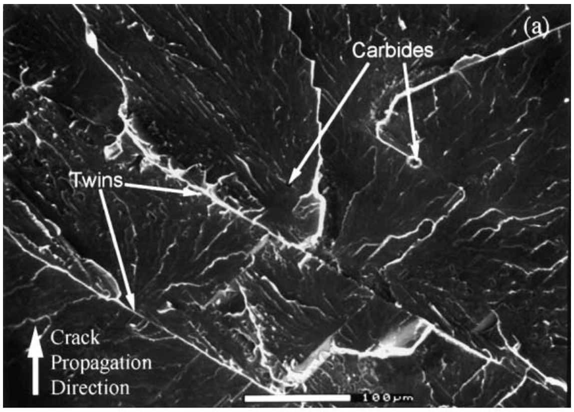

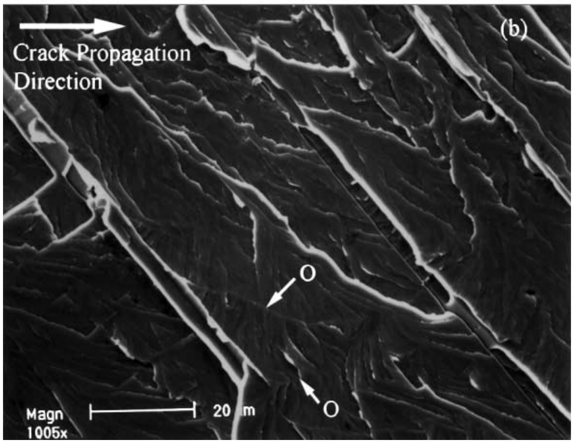

Fig. 9. SEM micrograph of fracture surface of grain A before decarburization showing repeated arrest and re-initiation of the cleavage crack by deformation twins (b) same observations after decarburization.

without decarburization, and one with decarburization respectively. Fig. 9a shows that the crack has been intercepted by the occasional large carbides. However, there are no significant emanations of cleavage river markings from these encounters, indicating that they have not played a significant role in the basic cleavage fracture. A much more significant interaction of the cleavage crack occurs with the deformation twins. There are many examples in both figures of repeated arrest of the cleavage crack by the narrow twins followed by points of break-through marked by river markings emanating form these points. Stereoscopic observations of the encounters of the crack with twins indicated that these repeated arrest and

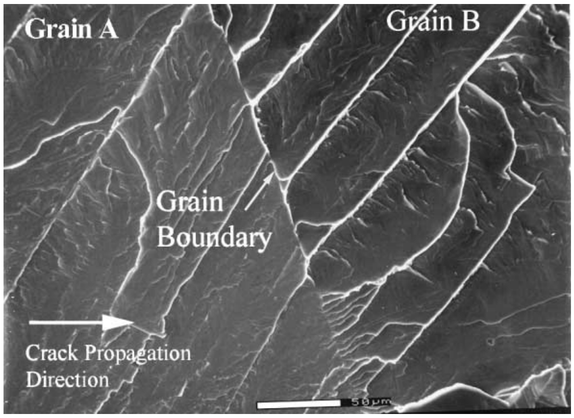

Fig. 10. SEM micrograph showing a "regular mode" of entry of a cleavage crack across a grain boundary into grain B along a series of twisted tiered cleavage strips in a specific case of bicrystal 14.

reinitiation events of the cleavage crack by twins, fragments the crack plane into separate strips advancing at different levels. Since the fracture toughness in cleavage-like fractures correlates well with the fracture surface roughness, this roughness was measured with a *Zygo Interferometer* [1] on several fracture surfaces of grain A in the low temperature range and was found to be of a rms roughness amplitude of 2.7 μm.

3.4.2. Fracture across grain boundaries at −20 °C

Detailed fractographic examination of the penetration of the cleavage crack from grain A across the boundary into grain B exhibited two limiting modes. Fig. 10 is a micrograph showing the dominant limiting mode identified as "regular", of entry of the cleavage crack from grain A into grain B in bicrystal 14 ($\psi = 21°$; $\varphi = 26°$). After initial arrest, and within the characteristic increment of crack tip driving force, as depicted in Fig. 5, the arrested cleavage crack front penetrates into grain B at a number of relatively evenly spaced points a characteristic distance w apart. The fully penetrated cleavage crack in grain B

[1] An instrument that uses scanning white light interferometry to image and measure the micro structure and topography of surfaces in three dimensions (New View System 5000, produced by Zygo Corp. of Middle-field, Connecticut).

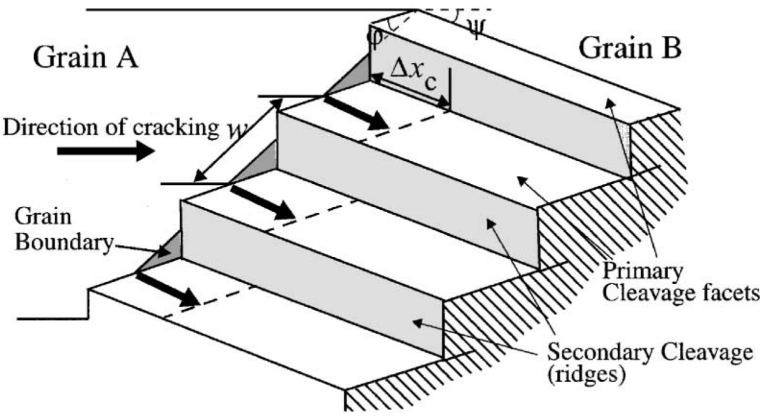

Fig. 11. Break-through of a cleavage crack across a grain boundary.

forms a series of "stair-case-like" tiers with flat surfaces of width $w/\cos\varphi$, with the twist inclination φ of the planes relative to the cleavage crack plane in grain A. In a transition region the individual cleavage facets bow into the designated strips from their entry points as depicted in Fig. 11, forming the tiered primary cleavage facets of grain B and in the process producing secondary cleavage-like fracture facets connecting up cleavage strips in grain B. At the critical condition the remaining grain boundary facets also give way by a combination of shear fracture or plastic shearing off, to complete the stair case type propagation of cleavage into grain B.

Since the distances w between the break-through points along a grain boundary on the cleavage plane of grain A, were judged to be an important dimension in assessing the penetration resistance of a grain boundary to cleavage cracks, the number distribution of the distances w was measured for three separate grain boundaries.

These boundaries identified as 13, 14 and 10 had systematically increasing angles of twist misorientations. Fig. 12a–c show these distributions of w spacings between break-through points along the cleavage crack. All three distributions show rather similar shapes which fitted reasonably well to a log–normal distribution function $p(x)$ given as

$$p(x) = \frac{1}{\sqrt{2\pi}\sigma x}\exp\left(-\frac{(\ln x-\mu)^2}{2\sigma^2}\right) \tag{9}$$

for $x > 0$, where $x = w/w_0$ represents a normalized length parameter, and the parameters σ and μ govern the shape of the distribution function, with $w_0 = 1.0 \times 10^{-6}$ m. The mean value $\bar{x}$ and the standard deviation s of the distributions are given by

$$\bar{x} = \exp\left[\tfrac{1}{2}(2\mu+\sigma^2)\right] \tag{10}$$

$$s = [\exp(2\mu+\sigma)^2(\exp\sigma^2-1)]^{1/2} \tag{11}$$

Specific evaluations of the distributions in samples 13 and 10 gave a peak value of the distribution in the range of roughly 2.5–3.0 μm for both sample 13 ($\bar{w} = 3.47$ μm; $s = 2.76$ μm) and for sample 10 ($\bar{w} = 5.18$ μm; $s = 4.12$ μm). The detailed examination of the ordering of these distances of break-through along the three individual boundaries, showed no important spatial clustering. There were no clear correlations between the distances w and the lattice twist misorientation angle, contrary to what might have been suspected. From these observations we conclude that the selection of the points of break-through by a cleavage crack along a grain boundary into the adjacent grain appears to be a random process, with the spacing w possibly depending only on a grain boundary structural feature.

Fig. 13 shows an example of an "irregular" penetration mode of the cleavage crack across the grain boundary in the bicrystal sample 13. In this case the cleavage crack has encountered the grain boundary first in a restricted region, and has

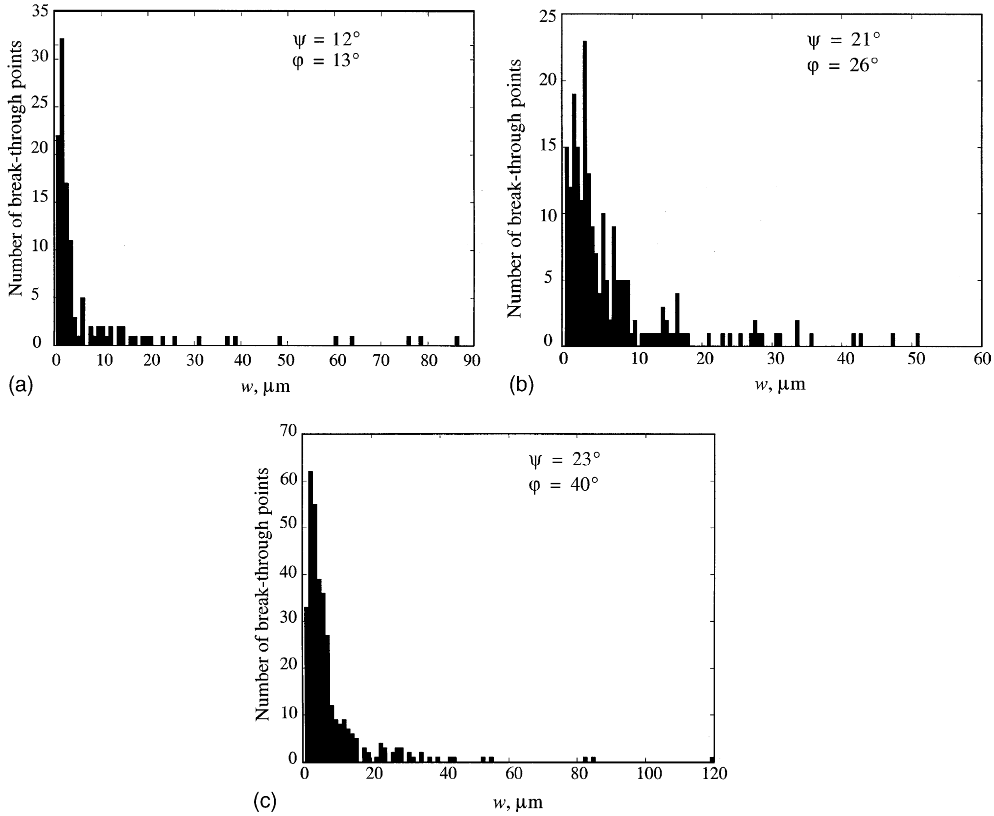

Fig. 12. Three specific determinations of the frequency distributions of the cleavage strip widths "w" in: (a) specimen 13 ($\psi = 12°$, $\varphi = 13°$); (b) specimen 14 ($\psi = 21°$, $\varphi = 26°$); (c) specimen 10 ($\psi = 23°$, $\varphi = 40°$).

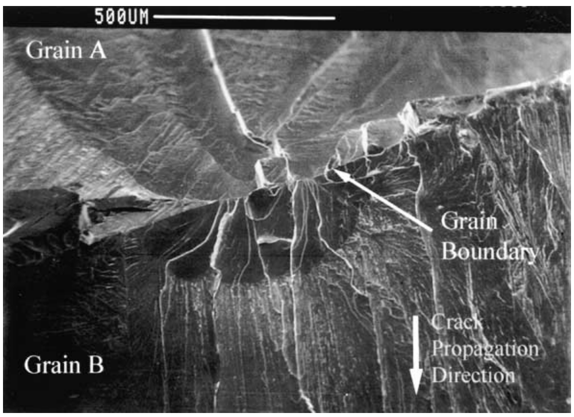

Fig. 13. SEM micrograph showing a case of an "irregular" mode of more localized break-through across a grain boundary.

penetrated across the boundary in a less regular form of entry points. As indicated by the river markings in grain B, the cleavage crack has then swung around and returned from grain B back to grain A, as depicted in the schematic of Fig. 14.

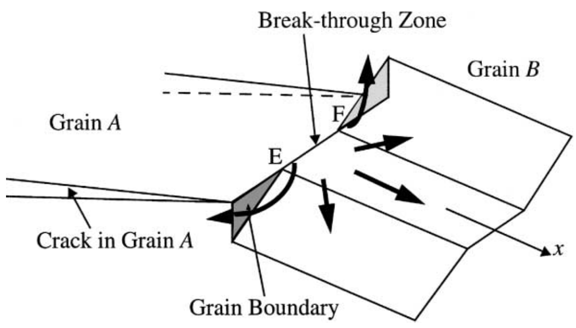

Fig. 14. Schematic showing an occasionally encountered case of local break-through of a grain boundary into grain B followed by return of the cleavage crack from grain B back into grain A.

3.4.3. Fractures across grain boundaries above the cleavage to mixed-cleavage transition

Fractographic observations of cleavage transition from grain A to grain B indicated very similar features with, however, a significant difference in the appearance of the cleavage fracture surface of grain B, shown in Fig. 15. The cleavage facets in grain B are produced in a very similar manner as depicted in the sketch of Fig. 11. There is, however, considerable undercutting at the overlap regions of the primary cleavage strips. Instead of the formation of secondary cleavage- like fracture facets, bridging the primary strips, the ligaments between strips have undergone considerable sigmoidal plastic bending as depicted in the sketch of Fig. 16 where the cleavage strips are viewed from grain B toward grain A. This suggests that a significant portion of the additional fracture work in the mixed-cleavage plateau does not occur at penetration of the grain boundary, but immediately subsequent to it, affecting the fracture work of grain B all along its length, but requiring a substantial initial increase in the rate of production of fracture work at the critical stage of break-through. These various fracture surface features encountered in the bicrystal penetration experiment have been found in abundance in the transit of cleavage cracks across grain boundaries in coarse-grained polycrystalline samples of Fe–2%Si alloy (Qiao and Argon, 2003).

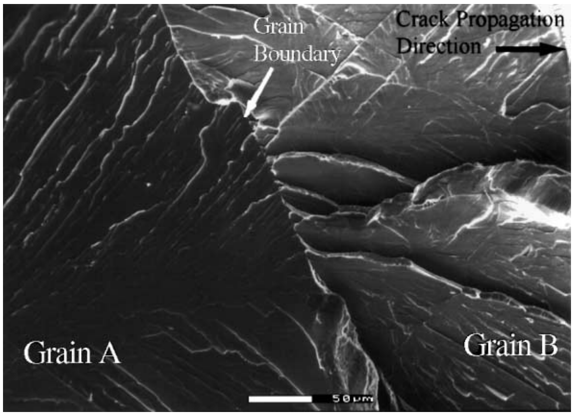

Fig. 15. SEM micrograph showing "undercutting" between adjacent cleavage strips, followed by sigmoidal plastic bending of connecting ligaments in grain B accounting for the increase in the break-through fracture work above the cleavage-to-mixed-cleavage transition.

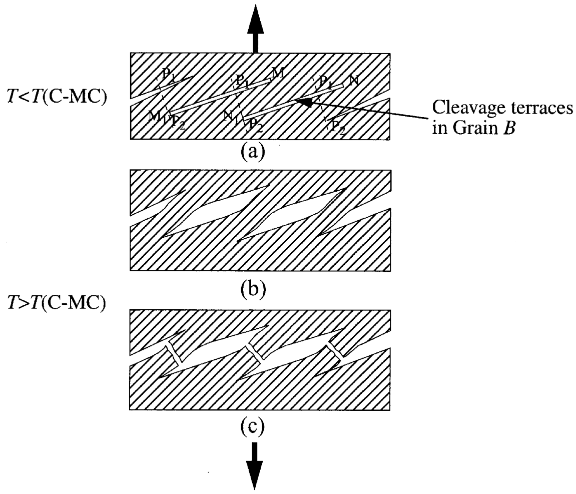

Fig. 16. Schematic depicting the connecting secondary cleavages between parallel cleavage strips in grain B below the cleavage-to-mixed-cleavage transition, and (b) and (c) above the c-to-mc transition with the sigmoidal plastic bending and rupture of connecting ligaments, as viewed from grain B toward grain A.

4. Models

4.1. Work of cleavage in a grain

As discussed above, the fracture toughness K_{ICA} of individual grains A of the bicrystal pairs, at −20 °C was found to be quite reproducible at an average level of 14.1 MPa $\sqrt{m}$ which converts to a very substantial work of fracture of $G_{ICA} = 850$ J/m^2 that requires explanation. Examination of the fracture surfaces in Fig. 9a and b shows only characteristic cleavage markings, but also much evidence of strong interactions of cleavage cracks with deformation twin bands resulting in periodic arrests and reinitiations of the cleavage cracking, and in the fragmentation of the cleavage plane into separate strips advancing at different levels as already pointed out above. There was considerable additional evidence, as shown e.g. in area "o" of Fig. 9b, of repeated weaker crack arrest, and re-initiation events resulting in the production of sets of smaller cleavage strips, indicating a very jerky nature of crack advance, modulated by the twins and possibly by other dislocation microstructure. The net effect of these crack plane shunting processes has resulted in a tiered fracture surface with an rms roughness of 2.7 μm as reported above. We view this fragmentation of the crack plane as the source of the substantial critical crack opening displacement δ_c associated with the crack advance.

In conventional interpretations of linear elastic fracture mechanics, in a small scale yielding setting, these measurements would be interpreted as having resulted from a quasi-statically advancing crack tip possessing a plastic zone of a radius $r_p \approx (1/\pi)(K_{ICA}/Y)^2$ ahead of it, and a critical crack opening displacement $\delta_p = r_p(Y/E)$ where Y would be the quasi-static tensile yield strength and E the Young's modulus. In the present case where the prevailing values are $Y = 0.25$ GPa, and $K_{ICA} = 14.1$ MPa$\sqrt{m}$, these expressions would give $r_p = 1.0$ mm and $\delta_c = 1.15$ μm respectively. While these estimates are not too unreasonable, the critical plastic zone size is somewhat too large and the opening displacement too small in comparison with expectations based on the fundamentally cleavage nature of the fracture surface features. Moreover, the development suggests a very conventional response of a plastic dissipation process preceeding the cleavage cracking as is typical in "upper shelf" cracking response, where the final cleavage separation in the previously plastically deformed zone is assumed to make only a negligible contribution to the overall fracture work.

In the present case where the temperature at −20 °C is roughly 270 °C below the conventional brittle-to-ductile transition temperature (Qiao and Argon, 2003), and the fracture surface features give much evidence of a jerky advance of a fragmented cleavage crack, far removed from a quasi-static response, we view the events of crack advance in a different order. We start by noting that the Fe–3%Si alloy is an intrinsically brittle solid, embrittled further by the high concentration of Si which is a potent-solid solution strengthening agent in Fe. When a "steady state" form of crack advance is established, with all its jerky features, as evidenced from the fracture surface markings of Fig. 9a and b, the average crack plane becomes fragmented, as discussed above, into a set of separate parallel cleavage strips. As depicted in Fig. 17, the separate cleavage strips of average width, w_n, are considered to penetrate into undeformed material at the tip of a process zone, (PZT), of extent Δ_c, without any accompanying plastic dissipation. This is in conformity with expectations from an intrinsically brittle solid well below its transition temperature where conditions of crack tip cleavage are reached well before conditions of plastic flow. As the cleavage strips of the PZT advance on planes randomly separated over a range δ_c, the edges of the strips that are left behind are subsequently bridged by processes of secondary cleavage-like fracture with plastic rubbing and some fragmentation. The major element of dissipative work is then done in the process zone of extent Δ_c until the two flanks of the rough cleavage crack are separated by the distance δ_c and all contact is terminated at point (CT), the crack tip. Such a process in which the inelastic dissipation is *subsequent* to the advancement of the cracking front resembles those frequently encountered in

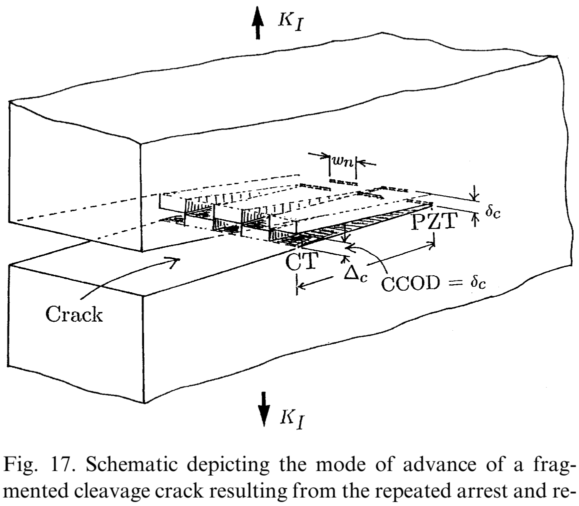

Fig. 17. Schematic depicting the mode of advance of a fragmented cleavage crack resulting from the repeated arrest and reinitiation phenomena of the crack by deformation twins. The fragmented cleavage cracks advance without accompanying plastic dissipation, while all plastic dissipation associated with the propagation is accomplished through the plastic shearing and rubbing of secondary cleavage surfaces within a critical process zone of extent Δ_c, subsequent to the critical cleavage penetration.

brittle composites reinforced with discrete fibers of a given length (δ_c) (Argon, 2000). The mechanics of the advance of such a process zone in which a characteristic traction separation (TS) process, illustrated in Fig. 18 is present and "processes" unbroken solid into fully separated crack flanks has been considered in detail by Andersson and Bergkvist (1970) (AB). We adapt our findings to their model. In that model which approximates the descending portion of the TS process law by a straight line over the separation distance CCOD $= \delta_c$, the critical process zone size Δ_c is given by

$$\Delta_c = \beta_c \frac{E}{\sigma_B}(\mathrm{CCOD}) \tag{12}$$

where the constant $\beta_c = 0.43$ is obtained from a numerical solution, σ_B is the average cohesive strength required to advance the cleavage front forward, and the CCOD is taken as the rms roughness range $\delta_c = 2.7 \times 10^{-6}$ m as measured here. With the prevailing parameters as given above, and taken σ_B as 1.0 GPa, the process zone size is estimated to be 2.5×10^{-4} m. Moreover, the AB model gives the essential work of fracture consisting of the inelastic dissipative processes along the process zone as

$$G_{\mathrm{ICA}} = \frac{\sigma_B(\mathrm{CCOD})}{2} \tag{13}$$

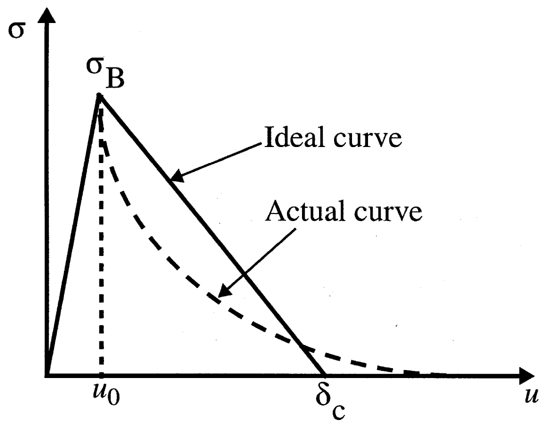

Fig. 18. An idealized traction separation TS profile demonstrating dissipative action in the process zone as proposed in the Andersson–Bergkvist model.

For the above chosen parameters G_{ICA} becomes 1350 J/m^2, or somewhat larger than the measured value of 850 J/m^2, with the discrepancy being readily accountable by a most probable drooping shape of the TS law, as depicted in Fig. 18. Finally, from these developments the cleavage strip width w_n can be calculated, as

$$w_n = \frac{Y(\mathrm{CCOD})^2}{2\sqrt{3}G_{\mathrm{ICA}}} \approx 0.62 \times 10^{-6}\ \mathrm{m} \tag{14}$$

for a tensile flow stress of $Y = 0.25$ GPa and a $G_{\mathrm{ICA}} = 850$ J/m^2, as measured experimentally. Where it is assumed that the inelastic dissipation occurs as plastic shearing.

While we prefer this interpretation of plastic dissipation *subsequent* to the initial cleavage penetration over the more conventional approach of cleavage *following* plastic dissipation, the actual behavior might be a combination of these two limiting responses.

4.2. Cleavage resistance model of grain boundaries

Referring to Fig. 10 representing the regular mode of penetration into the adjoining grain across the grain boundary and the schematic of Fig. 11, we view the sequence of processes of penetration of the cleavage crack up to the point of peak resistance as follows:

By a quasi-regular sampling process, the nature of which is not fully clear, the cleavage crack from grain A penetrates into grain B at points, on the average a distance w apart and spreads out on cleavage strips in grain B separated by distances $w \tan\varphi$, much like the early forms of penetration of brittle cracks between tough heterogeneities in a crack trapping model (Bower and Ortiz, 1991; Mower and Argon, 1995) with the as-yet-to-be sheared triangular grain boundary segments acting momentarily as the heterogeneities. Upon the penetration of the fragmented, terraced cleavage strips into grain B by increasing distances Δx, the opening displacements of the cleavage terraces begin to "force apart" the remaining triangular grain boundary islands to give way by a combination of plastic shear and shear cracking of the grain boundary over a relative shear displacement δ_B across the grain boundary faces that must depend on the distance of penetration Δx of the crack into grain B, i.e., $\delta_B = \beta\Delta x$. The remaining grain boundary islands finally give way completely when δ_B reaches a total displacement δ_{Bc}, at which time reaches Δx the critical level Δx_c where the maximum penetration resistance is reached.

The increase in the expanded energy ΔU required for overcoming the boundary resistance is, thus, made up of two components: (1) an increase in exposed cleavage surfaces along the terraces of width $w/\cos\varphi$ and the bridging cleavage-like processes that connect the terraces, and; (2) the grain boundary shear work expanded when a relative displacement δ_{Bc} takes place across the grain boundary plane. This gives

$$\Delta U = G_{ICA}\Delta A + \Delta W_p \tag{15}$$

$$\Delta A = \Delta x \frac{w}{(\cos\psi)^2}[\sin\varphi + \cos\varphi] \tag{16}$$

is the increment of cleavage surface with increasing average penetration distance Δx of the crack into grain B and where the tilt angle ψ and twist angle φ account for the geometrical projection effects of the actual cleavage surface area on the mean crack advance plane at the extension of the cleavage plane of grain A. We assume that the actual specific work of separation across this cleavage area remains to be G_{ICA} as in grain A. The increment of work of separation of the grain boundary islands sheared by the penetrating crack in grain B can be stated as

$$\Delta W_p = k\frac{\beta w^2 \Delta x}{4}\frac{\sin\varphi\cos\varphi}{\cos\psi} \tag{17}$$

At the point of maximum resistance of the boundary when Δx reaches Δx_c and δ_B reaches $\delta_{Bc} = \beta\Delta x_c$ the increment of expanded energy becomes

$$\Delta U = G_{ICA} w \Delta x_c \frac{1}{(\cos\psi)^2}(\sin\varphi + \cos\varphi) + k\frac{\beta w^2 \Delta x_c}{4}\frac{\sin\varphi\cos\varphi}{\cos\psi} \tag{18}$$

and the overall grain boundary break-through resistance becomes

$$G_{ICGB} = \frac{\Delta U}{w\Delta x_c} = G_{ICA}\frac{1}{(\cos\psi)^2}(\sin\varphi + \cos\varphi) + \frac{k\beta w}{4}\frac{\sin\varphi\cos\varphi}{\cos\psi} \tag{19}$$

giving the peak stress intensity to break-through of a grain boundary by pure cleavage

$$K_{ICGB} = \sqrt{\frac{EG_{ICGB}}{(1-\nu^2)}} \tag{20}$$

Finally, the differential cracking resistance of a grain boundary ΔK_{ICGB}, normalized with K_{ICA} gives a relatively simple expression as

$$\frac{\Delta K_{ICGB}}{K_{ICA}} = \sqrt{\frac{1}{(\cos\psi)^2}(\sin\varphi + \cos\varphi) + C\frac{\sin\varphi\cos\varphi}{\cos\psi}} - 1 \tag{21}$$

where the constant C

$$C = \frac{\beta k w}{4G_{ICA}} \tag{22}$$

is a material constant collecting together both some well known and some ill defined factors such as the coefficient β. The rest of Eq. (21) is of a purely geometrical nature. We note that when both ψ and φ go to zero Eq. (21) goes to zero, as it should.

We consider the parameter C as adjustable to obtain the best fit between the model and the experimental measurements for the 17 different bicrystal experiments by using experiment 13 with a contribution of substantial tilt and twist to fix C at 0.25. With this single fitting constant we have calculated the predictions of Eq. (21) for all 17 cases and compared the model predictions with the experimental measurements. The results given as a ratio $(\Delta K_{ICGB})_E/(\Delta K_{ICGB})_C$ of the experimental measurements to the computed values are presented in Table 2. While there is some scatter with the largest departure from unity being about 13%, the overall average ratio was found to be

$$(\Delta K_{ICGB})_E/(\Delta K_{ICGB})_C = 1.00 \pm 0.05 \tag{23}$$

which we consider to be quite good.

Using the most probable value of 2.5×10^{-6} m for w and $k = Y/\sqrt{3} = 0.144$ GPa, and $G_{ICA} = 850$ J/m^2, we estimate β to be 2.0 and, quite acceptable.

Pursuing the model further, we consider Eq. (21) also as a framework to calculate the boundary penetration resistance above the change to mixed-cleavage transition where considerable additional dissipative work is being done in the sigmoidal plastic bending of the ligaments connecting the individual cleavage strips in grain B. We consider this work formally associated with the grain boundary shear work, ΔW_p, of Eqs. (15) and (17). This is possible by a reinterpretation of the non-dimensional constant C in Eqs. (21) and (22). A new choice of C at a level of 1.70 also successfully takes account of the considerably larger break-through toughness for the two orientations "C" and "D" represented in Table 3.

Clearly, these fitting exercises demonstrate only a proper framework for considering the relative ordering of the measured parameters and does not constitute a fully definitive model.

5. Discussion

In the present bicrystal experiments we have demonstrated that the break-through of cleavage cracks across high angle grain boundaries is a topologically relatively simple process in the range well below the usual ductile-to-brittle fracture transition. In Fe–2%Si the latter transition in polycrystalline samples occurs for the usual compact experiment geometry at a temperature around 250 °C (Qiao and Argon, 2003). Thus, at −20 °C where most of our bicrystal experiments were performed the alloy under consideration is very brittle and the specific role of grain boundaries becomes relatively easily understandable. In our experiments we have found that the work of fracture (critical energy release rate) G_{ICA} of the well aligned starter grain A was in the range of 850 J/m^2 which is quite substantial. This high value of dissipated fracture work was explained by the presence of a longer range traction/separation relation arising from the fragmentation of the cleavage crack plane into parallel strips at different levels advancing separately but require bridging by additional plastic flow inside a process zone advancing with the crack.

How these considerations apply to the accounting of the cleavage resistance in polycrystals in the lower-shelf region is the subject for a separate communication (Qiao and Argon, 2003).

Acknowledgements

This research has been supported at its inception by the Materials Science Division of the ONR Under Grant N00014-96-1-0629 for which we are grateful to Dr. George Yoder. The research has been supported more recently by the NSF under Grant DMR-9906613. We also gratefully acknowledge receipt of two large blocks of Fe–3%Si alloy ingots from Allegheny Ludlum Steel Co. which made the bicrystal research possible. For this we are particularly grateful to Dr. James A. Salsgiver of the AL Technical Center.

Appendix A. Definition of relevant misorientation angles

The crystallographic reference axes should be those of grain A as shown in Fig. 2. By design of the experiment, axis **k** is parallel to the DCB load axis P and axis **j** is parallel to the wedge insertions axis, **x**. For the purpose of assessing the grain boundary resistance we consider a grain boundary that is nearly normal to the **x** axis, but actually its line of intersection with the cleavage plane of grain A makes an angle β with respect to the axis **i**. The boundary may also make an angle α relative to the axis **k**. For the purpose of the cleavage crack traversing from grain A to grain B the angle α is of much less importance. The crack growth resistance across the real boundary, making angles α and β should be almost indistinguishable from a reference plane perpendicular to the (0 0 1) plane that makes an angle β relative to axes **i** or **j**, i.e., a rotation about axis **k**. The tilt and twist angles ψ and φ of grain B should then be defined in relation to this virtual reference plane perpendicular to the (0 0 1) plane.

Grain B is misoriented relative to grain A. Its crystallographic axes $\mathbf{i}'$, $\mathbf{j}'$, and $\mathbf{k}'$ are defined by a set of direction cosines relative to the $\mathbf{i}$, $\mathbf{j}$, $\mathbf{k}$ axes of grain A. We make no distinction regarding the crack growth resistance in a cleavage plan, and treat the principal cleavage plane of grain B simply by its unit normal vector $\mathbf{n_B}$. We define the principal cleavage plane of grain B to be the one for which the unit normal vector $\mathbf{n_B}$ makes the smallest angle relative to the axis $\mathbf{k}$ of grain A. Therefore, $\mathbf{n_B}$ is parallel to axis $\mathbf{k}'$ of grain B. Thus,

$$\mathbf{n_B} = n_{B1}\mathbf{i} + n_{B2}\mathbf{j} + n_{B3}\mathbf{k} \tag{A.1}$$

referred to the principal axis of grain A. However, since $\mathbf{n_B}$ is parallel to $\mathbf{k}'$

$$\begin{aligned} n_{B1} &= \alpha_{31} \\ n_{B2} &= \alpha_{32} \\ n_{B3} &= \alpha_{33} \end{aligned} \tag{A.2}$$

where α_{31}, α_{32}, and α_{33} are the direction cosines of axis $\mathbf{k}'$ relative to the axis of grain A.

Consider now the virtual grain boundary plane, the line of intersection of which makes an angle β relative to axis $\mathbf{i}$. The plane is defined by a unit normal vector $\mathbf{b}$ which is given vectorially as

$$\mathbf{b} = b_1\mathbf{i} + b_2\mathbf{j} \quad (\text{with } b_3 = 0) \tag{A.3}$$

where

$$b_2 = \cos\beta, \quad b_1 = \sin\beta \tag{A.4}$$

in reality if the inclination is also considered, then $b_3 = \cos\alpha$ where α is the angle of rotation about the line of intersection of the virtual plane with the (0 0 1) plane, in the direction of axis $\mathbf{k}'$. We ignore this inclination for defining the principal tilt and twist angles of grain B relative to the plane of the virtual boundary.

Then, the principal tilt angles ψ and twist angle φ are redefined as follows.

$$\psi = \frac{\pi}{2} - a\cos(\mathbf{n_B}\mathbf{b}) \tag{A.5}$$

$$\varphi = \frac{\pi}{2} - a\cos(\mathbf{n_B}\mathbf{d}) \tag{A.6}$$

where $\mathbf{d}$ is the vector in the cleavage plane of grain A making an angle β with the $\mathbf{i}$ axis.

Then finally,

$$\psi = \frac{\pi}{2} - a\cos(\alpha_{31}\sin\beta + \alpha_{32}\cos\beta) \tag{A.7}$$

$$\varphi = \frac{\pi}{2} - a\cos(\alpha_{31}\cos\beta - \alpha_{32}\sin\beta) \tag{A.8}$$

if the boundary were perpendicular to axis $\mathbf{j}$ i.e., $\beta = 0$,

$$\psi = \frac{\pi}{2} - a\cos(\alpha_{32}) \tag{A.7a}$$

$$\varphi = \frac{\pi}{2} - a\cos(\alpha_{31}) \tag{A.8a}$$

References

Anderson, T.L., Stienstra, D., Dodds Jr, R.H., 1994. In: Landes, J.D., McCabe, D.E., Boulet, J.A.M. (Eds.), Fracture Mechanics: Twenty-Fourth Volume. In: ASTM STP-1207. ASTM, Philadelphia, PA, p. 186.

Andersson, H., Bergkvist, H., 1970. J. Mech. Phys. Solids 18, 1.

Argon, A.S., 2000. In: Kelly, A., Zweben, C. (Eds.), Comprehensive Composite Materials, vol. 1 (edited by Chou, T.-W.). Pergamon/Elsevier, Amsterdam, p. 763.

Birks, N., 1969. Decarburization. The Iron and Steel Inst, London.

Bower, A.F., Ortiz, M., 1991. J. Mech. Phys. Solids 39, 815.

Crocker, A., Smith, G., Flewitt, P., Moskovic, R., 1996. In: Proceedings of the 11th European Conference on Fracture (ECF11). Eng. Mater. Advis. Serv., Warley, UK, vol. 1. p. 233.

Gell, M., Smith, E., 1967. Acta Metall. 15, 253.

Hahn, G.T., Averbach, B.L., Owen, W.S., Cohen, M., 1959. In: Averbach, B.L., Felbeck, D.K., Hahn, G.T., Thomas, D.A. (Eds.), Fracture. MIT Press, Cambridge, MA, p. 91.

Hall, E.O., 1951. Proc. Phys. Soc. (London) B 64, 747.

Hull, D., 1960. Acta Metall. 8, 11.

Kanninen, M.F., 1973. Int. J. Fract. 9, 83.

Knott, J.F., 1997. In: Chan, K.S. (Ed.), Cleavage Fracture: George R. Irwin Symposium Proceedings. TMS, Warrendale, PA, p. 171.

Knott, J.F., Cottrell, A.H., 1963. J. Iron Steel Inst. 201, 249.

McClintock, F.A., 1997. In: Chan, K.S. (Ed.), Cleavage Fracture: George R. Irwin Symposium Proceedings. TMS, Warrendale, PA, p. 81.

McMahon, C.L., Cohen, M., 1965. Acta Metall. 13, 591.

Mower, T.M., Argon, A.S., 1995. Mech. Mater. 19, 343.

Petch, N.J., 1953. J. Iron Steel Inst. 174, 25.

Qiao, Y., Argon, A.S., 2003. Mech. Mater. 35, 129.

Ritchie, R.O., Knott, J.F., Rice, J.R., 1973. J. Mech. Phys. Solids 21, 395.

Stroh, A.N., 1954. Proc. Roy. Soc. (London) A 223, 404.

Stroh, A.N., 1955. Proc. Roy. Soc. (London) A 232, 548.

Thelning, K.E., 1984. Steel and Its Heat Treatment. Butterworth, London.

Zener, C., 1949. In: Fracturing of Metals. ASM, Metals Park, OH, p. 3.